

Inclusive transverse momentum distributions of charged particles in diffractive and non-diffractive photoproduction at HERA

ZEUS Collaboration

Abstract

Inclusive transverse momentum spectra of charged particles in photoproduction events in the laboratory pseudorapidity range $-1.2 < \eta < 1.4$ have been measured up to $p_T = 8$ GeV using the ZEUS detector. Diffractive and non-diffractive reactions have been selected with an average γp centre of mass (c.m.) energy of $\langle W \rangle = 180$ GeV. For diffractive reactions, the p_T spectra of the photon dissociation events have been measured in two intervals of the dissociated photon mass with mean values $\langle M_X \rangle = 5$ GeV and 10 GeV. The inclusive transverse momentum spectra fall exponentially in the low p_T region. The non-diffractive data show a pronounced high p_T tail departing from the exponential shape. The p_T distributions are compared to lower energy photoproduction data and to hadron-hadron collisions at a similar c.m. energy. The data are also compared to the results of a next-to-leading order QCD calculation.

The ZEUS Collaboration

M. Derrick, D. Krakauer, S. Magill, D. Mikunas, B. Musgrave, J. Repond, R. Stanek, R.L. Talaga, H. Zhang
Argonne National Laboratory, Argonne, IL, USA^p

R. Ayad¹, G. Bari, M. Basile, L. Bellagamba, D. Boscherini, A. Bruni, G. Bruni, P. Bruni, G. Cara Romeo,
G. Castellini², M. Chiarini, L. Cifarelli³, F. Cindolo, A. Contin, M. Corradi, I. Gialas⁴, P. Giusti, G. Iacobucci,
G. Laurenti, G. Levi, A. Margotti, T. Massam, R. Nania, C. Nemoz,
F. Palmonari, A. Polini, G. Sartorelli, R. Timellini, Y. Zamora Garcia¹, A. Zichichi
University and INFN Bologna, Bologna, Italy^f

A. Bargende, J. Crittenden, K. Desch, B. Diekmann⁵, T. Doeker, M. Eckert, L. Feld, A. Frey, M. Geerts,
G. Geitz⁶, M. Grothe, T. Haas, H. Hartmann, D. Haun⁵, K. Heinloth, E. Hilger,
H.-P. Jakob, U.F. Katz, S.M. Mari⁴, A. Mass⁷, S. Mengel, J. Mollen, E. Paul, Ch. Rembser, R. Schattevoy⁸,
D. Schramm, J. Stamm, R. Wedemeyer
Physikalisches Institut der Universität Bonn, Bonn, Federal Republic of Germany^c

S. Campbell-Robson, A. Cassidy, N. Dyce, B. Foster, S. George, R. Gilmore, G.P. Heath, H.F. Heath, T.J. Llewellyn,
C.J.S. Morgado, D.J.P. Norman, J.A. O'Mara, R.J. Tapper, S.S. Wilson, R. Yoshida
H.H. Wills Physics Laboratory, University of Bristol, Bristol, U.K.^o

R.R. Rau
Brookhaven National Laboratory, Upton, L.I., USA^p

M. Arneodo⁹, L. Iannotti, M. Schioppa, G. Susinno
Calabria University, Physics Dept. and INFN, Cosenza, Italy^f

A. Bernstein, A. Caldwell, N. Cartiglia, J.A. Parsons, S. Ritz¹⁰, F. Sciulli, P.B. Straub, L. Wai, S. Yang, Q. Zhu
Columbia University, Nevis Labs., Irvington on Hudson, N.Y., USA^q

P. Borzemiński, J. Chwastowski, A. Eskreys, K. Piotrkowski, M. Zachara, L. Zawiejski
Inst. of Nuclear Physics, Cracow, Poland^j

L. Adamczyk, B. Bednarek, K. Jeleń, D. Kisielewska, T. Kowalski, E. Rulikowska-Zarebska,
L. Suszycki, J. Zając
Faculty of Physics and Nuclear Techniques, Academy of Mining and Metallurgy, Cracow, Poland^j

A. Kotański, M. Przybycień
Jagellonian Univ., Dept. of Physics, Cracow, Poland^k

L.A.T. Bauerdick, U. Behrens, H. Beier¹¹, J.K. Bienlein, C. Coldewey, O. Deppe, K. Desler, G. Drews,
M. Flasiński¹², D.J. Gilkinson, C. Glasman, P. Göttlicher, J. Große-Knetter, B. Gutjahr, W. Hain, D. Hasell,
H. Heßling, Y. Iga, P. Joos, M. Kasemann, R. Klanner, W. Koch, L. Köpke¹³, U. Kötz, H. Kowalski, J. Labs,
A. Ladage, B. Löhr, M. Löwe, D. Lüke, O. Mańczak, T. Monteiro¹⁴, J.S.T. Ng, S. Nickel, D. Notz, K. Ohren-
berg, M. Roco, M. Rohde, J. Roldán, U. Schneekloth, W. Schulz, F. Selonke, E. Stiliaris¹⁵, B. Surov, T. Voß,
D. Westphal, G. Wolf, C. Youngman, J.F. Zhou
Deutsches Elektronen-Synchrotron DESY, Hamburg, Federal Republic of Germany

H.J. Grabosch, A. Kharchilava, A. Leich, M.C.K. Mattingly, A. Meyer, S. Schlenstedt, N. Wulff
DESY-Zeuthen, Inst. für Hochenergiephysik, Zeuthen, Federal Republic of Germany

G. Barbagli, P. Pelfer
University and INFN, Florence, Italy^f

G. Anzivino, G. Maccarrone, S. De Pasquale, L. Votano
INFN, Laboratori Nazionali di Frascati, Frascati, Italy^f

A. Bamberger, S. Eisenhardt, A. Freidhof, S. Söldner-Rembold¹⁶, J. Schroeder¹⁷, T. Trefzger
Fakultät für Physik der Universität Freiburg i.Br., Freiburg i.Br., Federal Republic of Germany^c

N.H. Brook, P.J. Bussey, A.T. Doyle¹⁸, J.I. Fleck⁴, D.H. Saxon, M.L. Utley, A.S. Wilson
Dept. of Physics and Astronomy, University of Glasgow, Glasgow, U.K. ^o

A. Dannemann, U. Holm, D. Horstmann, T. Neumann, R. Sinkus, K. Wick
Hamburg University, I. Institute of Exp. Physics, Hamburg, Federal Republic of Germany ^c

E. Badura¹⁹, B.D. Burow²⁰, L. Hagge, E. Lohrmann, J. Mainusch, J. Milewski, M. Nakahata²¹, N. Pavel,
G. Poelz, W. Schott, F. Zetsche
Hamburg University, II. Institute of Exp. Physics, Hamburg, Federal Republic of Germany ^c

T.C. Bacon, I. Butterworth, E. Gallo, V.L. Harris, B.Y.H. Hung, K.R. Long, D.B. Miller, P.P.O. Morawitz,
A. Priniias, J.K. Sedgbeer, A.F. Whitfield
Imperial College London, High Energy Nuclear Physics Group, London, U.K. ^o

U. Mallik, E. McCliment, M.Z. Wang, S.M. Wang, J.T. Wu, Y. Zhang
University of Iowa, Physics and Astronomy Dept., Iowa City, USA ^p

P. Cloth, D. Filges
Forschungszentrum Jülich, Institut für Kernphysik, Jülich, Federal Republic of Germany

S.H. An, S.M. Hong, S.W. Nam, S.K. Park, M.H. Suh, S.H. Yon
Korea University, Seoul, Korea ^h

R. Imlay, S. Kartik, H.-J. Kim, R.R. McNeil, W. Metcalf, V.K. Nadendla
Louisiana State University, Dept. of Physics and Astronomy, Baton Rouge, LA, USA ^p

F. Barreiro²², G. Cases, R. Graciani, J.M. Hernández, L. Hervás²², L. Labarga²², J. del Peso, J. Puga, J. Terron,
J.F. de Trocóniz
Univer. Autónoma Madrid, Depto de Física Teórica, Madrid, Spain ⁿ

G.R. Smith
University of Manitoba, Dept. of Physics, Winnipeg, Manitoba, Canada ^a

F. Corriveau, D.S. Hanna, J. Hartmann, L.W. Hung, J.N. Lim, C.G. Matthews, P.M. Patel,
L.E. Sinclair, D.G. Stairs, M. St-Laurent, R. Ullmann, G. Zacek
McGill University, Dept. of Physics, Montréal, Québec, Canada ^{a, b}

V. Bashkirov, B.A. Dolgoshein, A. Stifutkin
Moscow Engineering Physics Institute, Moscow, Russia ^l

G.L. Bashindzhagyan, P.F. Ermolov, L.K. Gladilin, Y.A. Golubkov, V.D. Kobrin, V.A. Kuzmin, A.S. Proskuryakov,
A.A. Savin, L.M. Shcheglova, A.N. Solomin, N.P. Zotov
Moscow State University, Institute of Nuclear Physics, Moscow, Russia ^m

M. Botje, F. Chlebana, A. Dake, J. Engelen, M. de Kamps, P. Kooijman, A. Kruse, H. Tiecke, W. Verkerke,
M. Vreeswijk, L. Wiggers, E. de Wolf, R. van Woudenberg
NIKHEF and University of Amsterdam, Netherlands ⁱ

D. Acosta, B. Bylsma, L.S. Durkin, K. Honscheid, C. Li, T.Y. Ling, K.W. McLean²³, W.N. Murray, I.H. Park,
T.A. Romanowski²⁴, R. Seidlein²⁵
Ohio State University, Physics Department, Columbus, Ohio, USA ^p

D.S. Bailey, G.A. Blair²⁶, A. Byrne, R.J. Cashmore, A.M. Cooper-Sarkar, D. Daniels²⁷,
R.C.E. Devenish, N. Harnew, M. Lancaster, P.E. Luffman²⁸, L. Lindemann⁴, J.D. McFall, C. Nath, V.A. Noyes,
A. Quadt, H. Uijterwaal, R. Walczak, F.F. Wilson, T. Yip
Department of Physics, University of Oxford, Oxford, U.K. ^o

G. Abbiendi, A. Bertolin, R. Brugnera, R. Carlin, F. Dal Corso, M. De Giorgi, U. Dosselli,
S. Limentani, M. Morandin, M. Posocco, L. Stanco, R. Stroili, C. Voci
Dipartimento di Fisica dell' Università and INFN, Padova, Italy ^f

J. Bulmahn, J.M. Butterworth, R.G. Feild, B.Y. Oh, J.J. Whitmore²⁹
Pennsylvania State University, Dept. of Physics, University Park, PA, USA^q

G. D'Agostini, G. Marini, A. Nigro, E. Tassi
Dipartimento di Fisica, Univ. 'La Sapienza' and INFN, Rome, Italy^f

J.C. Hart, N.A. McCubbin, K. Prytz, T.P. Shah, T.L. Short
Rutherford Appleton Laboratory, Chilton, Didcot, Oxon, U.K.^o

E. Barberis, T. Dubbs, C. Heusch, M. Van Hook, B. Hubbard, W. Lockman, J.T. Rahn,
H.F.-W. Sadrozinski, A. Seiden
University of California, Santa Cruz, CA, USA^p

J. Biltzinger, R.J. Seifert, A.H. Walenta, G. Zech
Fachbereich Physik der Universität-Gesamthochschule Siegen, Federal Republic of Germany^c

H. Abramowicz, G. Briskin, S. Dagan³⁰, A. Levy³¹
School of Physics, Tel-Aviv University, Tel Aviv, Israel^e

T. Hasegawa, M. Hazumi, T. Ishii, M. Kuze, S. Mine, Y. Nagasawa, M. Nakao, I. Suzuki, K. Tokushuku, S. Yamada,
Y. Yamazaki
Institute for Nuclear Study, University of Tokyo, Tokyo, Japan^g

M. Chiba, R. Hamatsu, T. Hirose, K. Homma, S. Kitamura, Y. Nakamitsu, K. Yamauchi
Tokyo Metropolitan University, Dept. of Physics, Tokyo, Japan^g

R. Cirio, M. Costa, M.I. Ferrero, L. Lamberti, S. Maselli, C. Peroni, R. Sacchi, A. Solano, A. Staiano
Universita di Torino, Dipartimento di Fisica Sperimentale and INFN, Torino, Italy^f

M. Dardo
II Faculty of Sciences, Torino University and INFN - Alessandria, Italy^f

D.C. Bailey, D. Bandyopadhyay, F. Benard, M. Brkic, M.B. Crombie, D.M. Gingrich³², G.F. Hartner, K.K. Joo,
G.M. Levman, J.F. Martin, R.S. Orr, C.R. Sampson, R.J. Teuscher
University of Toronto, Dept. of Physics, Toronto, Ont., Canada^a

C.D. Catterall, T.W. Jones, P.B. Kaziewicz, J.B. Lane, R.L. Saunders, J. Shulman
University College London, Physics and Astronomy Dept., London, U.K.^o

K. Blankenship, B. Lu, L.W. Mo
Virginia Polytechnic Inst. and State University, Physics Dept., Blacksburg, VA, USA^q

W. Bogusz, K. Charchuła, J. Ciborowski, J. Gajewski, G. Grzelak, M. Kasprzak, M. Krzyżanowski,
K. Muchorowski, R.J. Nowak, J.M. Pawlak, T. Tymieniecka, A.K. Wróblewski, J.A. Zakrzewski, A.F. Żarnecki
Warsaw University, Institute of Experimental Physics, Warsaw, Poland^j

M. Adamus
Institute for Nuclear Studies, Warsaw, Poland^j

Y. Eisenberg³⁰, U. Karshon³⁰, D. Revel³⁰, D. Zer-Zion
Weizmann Institute, Nuclear Physics Dept., Rehovot, Israel^d

I. Ali, W.F. Badgett, B. Behrens, S. Dasu, C. Fordham, C. Foudas, A. Goussiou, R.J. Loveless, D.D. Reeder,
S. Silverstein, W.H. Smith, A. Vaiciulis, M. Wodarczyk
University of Wisconsin, Dept. of Physics, Madison, WI, USA^p

T. Tsurugai
Meiji Gakuin University, Faculty of General Education, Yokohama, Japan

S. Bhadra, M.L. Cardy, C.-P. Fagerstroem, W.R. Frisken, K.M. Furutani, M. Khakzad, W.B. Schmidke
York University, Dept. of Physics, North York, Ont., Canada^a

¹ supported by Worldlab, Lausanne, Switzerland
² also at IROE Florence, Italy
³ now at Univ. of Salerno and INFN Napoli, Italy
⁴ supported by EU HCM contract ERB-CHRX-CT93-0376
⁵ now a self-employed consultant
⁶ on leave of absence
⁷ now at Institut für Hochenergiephysik, Univ. Heidelberg
⁸ now at MPI Berlin
⁹ now also at University of Torino
¹⁰ Alfred P. Sloan Foundation Fellow
¹¹ presently at Columbia Univ., supported by DAAD/HSPH-AUFE
¹² now at Inst. of Computer Science, Jagellonian Univ., Cracow
¹³ now at Univ. of Mainz
¹⁴ supported by DAAD and European Community Program PRAXIS XXI
¹⁵ supported by the European Community
¹⁶ now with OPAL Collaboration, Faculty of Physics at Univ. of Freiburg
¹⁷ now at SAS-Institut GmbH, Heidelberg
¹⁸ also supported by DESY
¹⁹ now at GSI Darmstadt
²⁰ also supported by NSERC
²¹ now at Institute for Cosmic Ray Research, University of Tokyo
²² on leave of absence at DESY, supported by DGICYT
²³ now at Carleton University, Ottawa, Canada
²⁴ now at Department of Energy, Washington
²⁵ now at HEP Div., Argonne National Lab., Argonne, IL, USA
²⁶ now at RHBNC, Univ. of London, England
²⁷ Fulbright Scholar 1993-1994
²⁸ now at Cambridge Consultants, Cambridge, U.K.
²⁹ on leave and partially supported by DESY 1993-95
³⁰ supported by a MINERVA Fellowship
³¹ partially supported by DESY
³² now at Centre for Subatomic Research, Univ. of Alberta, Canada and TRIUMF, Vancouver, Canada

^a supported by the Natural Sciences and Engineering Research Council of Canada (NSERC)
^b supported by the FCAR of Québec, Canada
^c supported by the German Federal Ministry for Research and Technology (BMFT)
^d supported by the MINERVA Gesellschaft für Forschung GmbH, and by the Israel Academy of Science
^e supported by the German Israeli Foundation, and by the Israel Academy of Science
^f supported by the Italian National Institute for Nuclear Physics (INFN)
^g supported by the Japanese Ministry of Education, Science and Culture (the Monbusho) and its grants for Scientific Research
^h supported by the Korean Ministry of Education and Korea Science and Engineering Foundation
ⁱ supported by the Netherlands Foundation for Research on Matter (FOM)
^j supported by the Polish State Committee for Scientific Research (grant No. SPB/P3/202/93) and the Foundation for Polish- German Collaboration (proj. No. 506/92)
^k supported by the Polish State Committee for Scientific Research (grant No. PB 861/2/91 and No. 2 2372 9102, grant No. PB 2 2376 9102 and No. PB 2 0092 9101)
^l partially supported by the German Federal Ministry for Research and Technology (BMFT)
^m supported by the German Federal Ministry for Research and Technology (BMFT), the Volkswagen Foundation, and the Deutsche Forschungsgemeinschaft
ⁿ supported by the Spanish Ministry of Education and Science through funds provided by CICYT
^o supported by the Particle Physics and Astronomy Research Council
^p supported by the US Department of Energy
^q supported by the US National Science Foundation

1 Introduction

HERA is a prodigious source of quasi-real photons from reactions where the electron is scattered at very small angles. This permits the study of photoproduction reactions at photon-proton centre of mass (c.m.) energies an order of magnitude larger than in previous fixed target experiments.

The majority of the γp collisions are due to interactions of the proton with the hadronic structure of the photon, a process that has been successfully described by the vector meson dominance model (VDM)[1]. Here, the photon is pictured to fluctuate into a virtual vector meson that subsequently collides with the proton. Such collisions exhibit the phenomenological characteristics of hadron-hadron interactions. In particular they can proceed via diffractive or non-diffractive channels. The diffractive interactions are characterized by very small four momentum transfers and no colour exchange between the colliding particles leading to final states where the colliding particles appear either intact or as more massive dissociated states. However, it has been previously demonstrated that photoproduction collisions at high transverse momentum cannot be described solely in terms of the fluctuation of the photon into a hadron-like state [2, 3]. The deviations come from contributions of two additional processes called direct and anomalous. In the former process the photon couples directly to the charged partons inside the proton. The anomalous component corresponds to the process where the photon couples to a $q\bar{q}$ pair without forming a bound state. The interactions of the photon via the hadron-like state and the anomalous component are referred to as resolved photoproduction, since both of them can be described in terms of the partonic structure of the photon [4].

In this paper we present the measurement of the transverse momentum spectra of charged particles produced in photoproduction reactions at an average c.m. energy of $\langle W \rangle = 180$ GeV and in the laboratory pseudorapidity range $-1.2 < \eta < 1.4$ ¹. This range approximately corresponds to the c.m. pseudorapidity interval of $0.8 < \eta_{c.m.} < 3.4$, where the direction is defined such that positive $\eta_{c.m.}$ values correspond to the photon fragmentation region. The transverse momentum distributions of charged particles are studied for non-diffractive and diffractive reactions separately. The p_T spectrum from non-diffractive events is compared to low energy photoproduction data and to hadron-hadron collisions at a similar c.m. energy. In the region of high transverse momenta we compare the data to the predictions of a next-to-leading order QCD calculation.

The diffractive reaction ($\gamma p \rightarrow Xp$), where X results from the dissociation of the photon, was previously measured by the E612 Fermilab experiment at much lower c.m. energies, $11.8 < W < 16.6$ GeV [5]. It was demonstrated that the properties of the diffractive excitation of the photon resemble diffraction of hadrons in terms of the distribution of the dissociated mass, the distribution of the four-momentum transfer between the colliding objects [5] and the ratio of the diffractive cross section to the total cross section [6]. The hadronization of diffractively dissociated photons has not yet been systematically studied. In this analysis we present the measurement of inclusive p_T spectra in two intervals of the dissociated photon mass with mean values of $\langle M_X \rangle = 5$ GeV and $\langle M_X \rangle = 10$ GeV.

¹Pseudorapidity η is calculated from the relation $\eta = -\ln(\tan(\theta/2))$, where θ is a polar angle calculated with respect to the proton beam direction.

2 Experimental setup

The analysis is based on data collected with the ZEUS detector in 1993, corresponding to an integrated luminosity of 0.40 pb^{-1} . The HERA machine was operating at an electron energy of 26.7 GeV and a proton energy of 820 GeV, with 84 colliding bunches. In addition 10 electron and 6 proton bunches were left unpaired for background studies (pilot bunches).

A detailed description of the ZEUS detector may be found elsewhere [7, 8]. Here, only a brief description of the detector components used for this analysis is given. Throughout this paper the standard ZEUS right-handed coordinate system is used, which has its origin at the nominal interaction point. The positive Z-axis points in the direction of the proton beam, called the forward direction, and X points towards the centre of the HERA ring.

Charged particles created in ep collisions are tracked by the inner tracking detectors which operate in a magnetic field of 1.43 T provided by a thin superconducting solenoid. Immediately surrounding the beampipe is the vertex detector (VXD), a cylindrical drift chamber which consists of 120 radial cells, each with 12 sense wires running parallel to the beam axis [9]. The achieved resolution is $50 \mu\text{m}$ in the central region of a cell and $150 \mu\text{m}$ near the edges. Surrounding the VXD is the central tracking detector (CTD) which consists of 72 cylindrical drift chamber layers organized in 9 superlayers [10]. These superlayers alternate between those with wires parallel to the collision axis and those with wires inclined at a small angle to provide a stereo view. The magnetic field is significantly inhomogeneous towards the ends of the CTD thus complicating the electron drift. With the present understanding of the chamber, a spatial resolution of $\approx 260 \mu\text{m}$ has been achieved. The hit efficiency of the chamber is greater than 95%.

In events with charged particle tracks, using the combined data from both chambers, the position resolution of the reconstructed primary vertex are 0.6 cm in the Z direction and 0.1 cm in the XY plane. The resolution in transverse momentum for full length tracks is $\sigma_{p_T}/p_T \leq 0.005 \cdot p_T \oplus 0.016$ (p_T in GeV). The description of the track and the vertex reconstruction algorithms may be found in [11] and references therein.

The solenoid is surrounded by the high resolution uranium-scintillator calorimeter (CAL) divided into the forward (FCAL), barrel (BCAL) and rear (RCAL) parts [12]. Holes of $20 \times 20 \text{ cm}^2$ in the centre of FCAL and RCAL are required to accommodate the HERA beam pipe. Each of the calorimeter parts is subdivided into towers which in turn are segmented longitudinally into electromagnetic (EMC) and hadronic (HAC) sections. These sections are further subdivided into cells, which are read out by two photomultiplier tubes. Under test beam conditions, an energy resolution of the calorimeter of $\sigma_E/E = 0.18/\sqrt{E}$ (GeV) for electrons and $\sigma_E/E = 0.35/\sqrt{E}$ (GeV) for hadrons was measured. In the analysis presented here CAL cells with an EMC (HAC) energy below 60 MeV (110 MeV) are excluded to minimize the effect of calorimeter noise. This noise is dominated by uranium activity and has an r.m.s. value below 19 MeV for EMC cells and below 30 MeV for HAC cells.

The luminosity detector (LUMI) measures the rate of the Bethe-Heitler process $ep \rightarrow e\gamma p$. The detector consists of two lead-scintillator sandwich calorimeters installed in the HERA tunnel and is designed to detect electrons scattered at very small angles and photons emitted along the electron beam direction [13]. Signals in the LUMI electron calorimeter are used to tag events and to measure the energy of the interacting photon, E_γ , from $E_\gamma = E_e - E'_e = 26.7 \text{ GeV} - E'_e$, where E'_e is the energy measured in the LUMI.

3 Trigger

The events used in the following analysis were collected using a trigger requiring a coincidence of the signals in the LUMI electron calorimeter and in the central calorimeter. The small angular acceptance of the LUMI electron calorimeter implied that in all the triggered events the virtuality of the exchanged photon was between $4 \cdot 10^{-8} < Q^2 < 0.02 \text{ GeV}^2$.

The central calorimeter trigger required an energy deposit in the RCAL EMC section of more than 464 MeV (excluding the towers immediately adjacent to the beam pipe) or 1250 MeV (including those towers). In addition we also used the events triggered by an energy in the BCAL EMC section exceeding 3400 MeV. At the trigger level the energy was calculated using only towers with more than 464 MeV of deposited energy.

4 Event selection

In the offline analysis the energy of the scattered electron detected in the LUMI calorimeter was required to satisfy $15.2 < E'_e < 18.2 \text{ GeV}$, limiting the γp c.m. energy to the interval $167 < W < 194 \text{ GeV}$. The longitudinal vertex position determined from tracks was required to be $-35 \text{ cm} < Z_{\text{vertex}} < 25 \text{ cm}$. The vertex cut removed a substantial part of the beam gas background and limited the data sample to the region of uniform detector acceptance. The cosmic ray background was suppressed by requiring the transverse momentum imbalance of the deposits in the main calorimeter, P_{missing} , relative to the square root of the total transverse energy, $\sqrt{E_T}$, to be small: $P_{\text{missing}}/\sqrt{E_T} < 2\sqrt{\text{GeV}}$.

The data sample was divided into a diffractive and a non-diffractive subset according to the pseudorapidity, η_{max} , of the most forward energy deposit in the FCAL with energy above 400 MeV. The requirement of $\eta_{\text{max}} < 2$ selects events with a pronounced rapidity gap that are predominantly due to diffractive processes ($\approx 96\%$ according to Monte Carlo (MC) simulation, see section 6). The events with $\eta_{\text{max}} > 2$ are almost exclusively ($\approx 95\%$) due to non-diffractive reactions. The final non-diffractive data sample consisted of 149500 events.

For the diffractive data sample ($\eta_{\text{max}} < 2$) an additional cut $\eta_{\text{max}} > -2$ was applied to suppress the production of light vector mesons V in the diffractive reactions $\gamma p \rightarrow Vp$ and $\gamma p \rightarrow VN$, where N denotes a nucleonic system resulting from the dissociation of the proton. The remaining sample was analyzed as a function of the mass of the dissociated system reconstructed from the empirical relationship

$$M_{X_{\text{rec}}} \approx A \cdot \sqrt{E^2 - P_Z^2} + B = A \cdot \sqrt{(E + P_Z) \cdot E_\gamma} + B.$$

The above formula exploits the fact that in tagged photoproduction the diffractively excited photon state has a relatively small transverse momentum. The total hadronic energy, E , and longitudinal momentum $P_Z = E \cdot \cos\theta$ were measured with the uranium calorimeter by summing over all the energy deposits of at least 160 MeV. The correction factors $A = 1.7$ and $B = 1.0 \text{ GeV}$ compensate for the effects of energy loss in the inactive material, beam pipe holes, and calorimeter cells that failed the energy threshold cuts. The formula was optimized to give the best approximation of the true invariant mass in diffractive photon dissociation events obtained from MC simulations, while being insensitive to the calorimeter noise. The diffractive data were analyzed in two intervals of the reconstructed mass, namely $4 < M_{X_{\text{rec}}} < 7 \text{ GeV}$ and $8 < M_{X_{\text{rec}}} < 13 \text{ GeV}$. According to the MC simulation the first cut selects events generated with a mass having a mean value and spread of $\langle M_{X_{\text{GEN}}} \rangle = 5 \text{ GeV}$ and r.m.s. = 1.8 GeV. The

second cut results in $\langle M_{XGEN} \rangle = 10$ GeV and r.m.s. = 2.3 GeV. Details of the MC simulation are given in section 6. The final data sample consisted of 5123 events in the lower M_X interval and of 2870 events in the upper interval.

The contamination of the final data samples from e–gas background ranges from $< 0.1\%$ (non-diffractive sample) to $\approx 10\%$ (diffractive sample, $\langle M_X \rangle = 5$ GeV). The p–gas contribution is between 1% (non-diffractive sample) and 2% (diffractive sample, $\langle M_X \rangle = 5$ GeV). The e–gas background was statistically subtracted using the electron pilot bunches. A similar method was used to correct for the p–gas background that survived the selection cuts because of an accidental coincidence with an electron bremsstrahlung ($ep \rightarrow \gamma ep$). A large fraction of these background events were identified using the LUMI detector, since the energy deposits in the electron and photon calorimeters summed up to the electron beam energy. The identified background events were included with negative weights into all of the distributions in order to compensate for the unidentified part of the coincidence background. A detailed description of the statistical background subtraction method may be found in [6, 14].

5 Track selection

The charged tracks used for this analysis were selected with the following criteria:

- only tracks accepted by an event vertex fit were selected. This eliminated most of the tracks that came from secondary interactions and decays of short lived particles;
- tracks must have hits in each of the first 5 superlayers of the CTD. This requirement ensures that only long, well reconstructed tracks are used for the analysis;
- $-1.2 < \eta < 1.4$ and $p_T > 0.3$ GeV. These two cuts select the region of high acceptance of the CTD where the detector response and systematics are best understood.

Using Monte Carlo events, we estimated that the efficiency of the charged track reconstruction convoluted with the acceptance of the selection cuts is about 90% and is uniform in p_T . The contamination of the final sample from secondary interaction tracks, products of decays of short lived particles, and from spurious tracks (artifacts of the reconstruction algorithm) ranges from 5% at $p_T = 0.3$ GeV to 3% for $p_T > 1$ GeV. The inefficiency and remaining contamination of the final track sample is accounted for by the acceptance correction described in the following section.

The transverse momenta of the measured tracks displayed no correlation with η over the considered interval and were symmetric with respect to the charge assigned to the track.

6 Monte Carlo models

For the acceptance correction and selection cut validation we used Monte Carlo events generated with a variety of programs. Soft, non-diffractive collisions of the proton with a VDM type photon were generated using HERWIG 5.7 with the minimum bias option [15]. The generator was tuned to fit the ZEUS data on charged particle multiplicity and transverse energy distributions. For the evaluation of the model dependence of our measurements we also used events from the PYTHIA generator with the soft hadronic interaction option [16]. Hard resolved and direct subprocesses were simulated using the standard HERWIG 5.7 generator with the lower cut-off on the transverse momentum of the final-state partons, p_{Tmin} , chosen to be

2.5 GeV. For the parton densities of the colliding particles, the GRV-LO [17] (for the photon) and MRSD' [18] (for the proton) parametrisations were used. As a cross-check we also used hard γp scattering events generated by PYTHIA with $p_{Tmin} = 5$ GeV. The soft and hard MC components were combined in a ratio that gave the best description of the transverse momentum distribution of the track with the largest p_T in each event. For $p_{Tmin} = 2.5$ GeV, the hard component comprises 11% of the non-diffractive sample and for $p_{Tmin} = 5$ GeV only about 3%. Each diffractive subprocess was generated separately. The diffractive production of vector mesons (ρ, ω, ϕ) was simulated with PYTHIA. The same program was used to simulate the double diffractive dissociation ($\gamma p \rightarrow XN$). The diffractive excitation of the photon ($\gamma p \rightarrow Xp$) was generated with the EPDIF program which models the diffractive system as a quark-antiquark pair produced along the collision axis [19]. Final state QCD radiation and hadronization were simulated using JETSET [16]. For the study of systematic uncertainties, a similar sample of events was obtained by enriching the standard PYTHIA diffractive events with the hard component simulated using the POMPYT Monte Carlo program (hard, gluonic pomeron with the direct photon option) [20].

The MC samples corresponding to the diffractive subprocesses were combined with the non-diffractive component in the proportions given by the ZEUS measurement of the partial photoproduction cross sections [6]. The MC events were generated without electroweak radiative corrections. In the considered W range, the QED radiation effects result in $\approx 2\%$ change in the number of measured events so that the effect on the results of this analysis are negligible. The generated events were processed through the detector and trigger simulation programs and run through the standard ZEUS reconstruction chain.

7 Acceptance correction

The acceptance corrected transverse momentum spectrum was derived from the reconstructed spectrum of charged tracks, by means of a multiplicative correction factor, calculated using Monte Carlo techniques:

$$C(p_T) = \left(\frac{1}{N_{gen\ ev}} \cdot \frac{dN_{gen}}{dp_{Tgen}} \right) / \left(\frac{1}{N_{rec\ ev}} \cdot \frac{dN_{rec}}{dp_{Trec}} \right).$$

N_{gen} denotes the number of primary charged particles generated with a transverse momentum p_{Tgen} in the considered pseudorapidity interval and $N_{gen\ ev}$ is the number of generated events. Only the events corresponding to the appropriate type of interaction were included, e.g. for the lower invariant mass interval of the diffractive sample only the Monte Carlo events corresponding to diffractive photon dissociation with the generated invariant mass $4 < M_{Xgen} < 7$ GeV were used. N_{rec} is the number of reconstructed tracks passing the experimental cuts with a reconstructed transverse momentum of p_{Trec} , while $N_{rec\ ev}$ denotes the number of events used. Only the events passing the trigger simulation and the experimental event selection criteria were included in the calculation. To account for the contribution of all the subprocesses, the combination of the MC samples described in section 6 was used.

This method corrects for the following effects in the data:

- the limited trigger acceptance;
- the inefficiencies of the event selection cuts, in particular the contamination of the diffractive spectra from non-diffractive processes and the events with a dissociated mass that

was incorrectly reconstructed. Also the non-diffractive sample is corrected for the contamination from diffractive events with high dissociated mass;

- limited track finding efficiency and acceptance of the track selection cuts, as well as the limited resolution in momentum and angle;
- loss of tracks due to secondary interactions and contamination from secondary tracks;
- decays of charged pions and kaons, photon conversions and decays of lambdas and neutral kaons. Thus, in the final spectra the charged kaons appear, while the decay products of neutral kaons and lambdas do not. For all the other strange and charmed states, the decay products were included.

The validity of our acceptance correction method relies on the correct simulation of the described effects in the Monte Carlo program. The possible discrepancies between reality and Monte Carlo simulation were analyzed and the estimation of the effect on the final distributions was included in the systematic uncertainty, as described in the following section.

8 Systematic effects

One of the potential sources of systematic inaccuracy is the tracking system and its simulation in the Monte Carlo events used for the acceptance correction. Using an alternative simulation code with artificially degraded tracking performance we verified that the efficiency to find a track which fulfills all the selection cuts is known with an accuracy of about 10%. The error due to an imprecise description of the momentum resolution at high p_T is negligible compared to the statistical precision of the data. We also verified that the final spectra would not change significantly if the tracking resolution at high p_T had non-gaussian tails at the level of 10% or if the measured momentum was systematically shifted from the true value by the momentum resolution.

Another source of systematic uncertainty is the Monte Carlo simulation of the trigger response. We verified that even a very large (20%) inaccuracy of the BCAL energy threshold would not produce a statistically significant effect. An incorrect RCAL trigger simulation would change the number of events observed, but would not affect the final p_T spectra since it is normalized to the number of events. The correlation between the RCAL energy and the p_T of tracks is very small.

To evaluate the model dependence we repeated the calculation of the correction factors using an alternative set of Monte Carlo programs (see section 6) and compared the results with the original ones. The differences between the obtained factors varied between 5% for the high mass diffractive sample and 11% for the non-diffractive one. The sensitivity of the result to the assumed relative cross sections of the physics processes was checked by varying the subprocess ratios within the error limits given in [6]. The effect was at most 3%.

All the above effects were combined in quadrature, resulting in an overall systematic uncertainty of the charged particle rates as follows: 15% in the non-diffractive sample, 15% in the $\langle M_X \rangle = 5\text{GeV}$ diffractive sample and 9% in the $\langle M_X \rangle = 10\text{GeV}$ diffractive sample. All these systematic errors are independent of p_T .

9 Results

The double differential rate of charged particle production in an event of a given type is calculated as the number of charged particles ΔN produced within $\Delta\eta$ and Δp_T in N_{ev} events as a function of p_T :

$$\frac{1}{N_{ev}} \cdot \frac{d^2 N}{dp_T^2 d\eta} = \frac{1}{N_{ev}} \cdot \frac{1}{2p_T \Delta\eta} \cdot \frac{\Delta N}{\Delta p_T}.$$

The charged particle transverse momentum spectrum was derived from the transverse momentum distribution of observed tracks normalized to the number of data events by means of the correction factor described in section 7. The resulting charged particle production rates in diffractive and non-diffractive events are presented in Fig. 1 and listed in Tables 1, 2 and 3. In the figure the inner error bars indicate the statistical error. Quadratically combined statistical and systematic uncertainties are shown as the outer error bars. The $\langle M_X \rangle = 5$ GeV diffractive spectrum extends to $p_T = 1.75$ GeV and the $\langle M_X \rangle = 10$ GeV distribution extends to $p_T = 2.5$ GeV. The non-diffractive distribution falls steeply in the low p_T region but lies above the exponential fit at higher p_T values. The measurements extend to $p_T = 8$ GeV.

The soft interactions of hadrons can be successfully described by thermodynamic models that predict a steep fall of the transverse momentum spectra that can be approximated with the exponential form [21]:

$$\frac{1}{N_{ev}} \cdot \frac{d^2 N}{dp_T^2 d\eta} = \exp(a - b \cdot \sqrt{p_T^2 + m_\pi^2}) \quad (1)$$

where m_π is the pion mass. The results of the fits of this function to ZEUS data in the interval $0.3 < p_T < 1.2$ GeV are also shown as the full line in Fig. 1. The resulting values of the exponential slope b are listed in Table 4. The systematic errors were estimated by varying the relative inclusive cross sections within the systematic error limits (see section 8) and by varying the upper boundary of the fitted interval from $p_T = 1.0$ GeV to 1.4 GeV.

In Fig. 2 we present a comparison of the b parameter resulting from the fits of (1) to proton-proton and proton-antiproton data as a function of the c.m. energy. The slope of the ZEUS non-diffractive spectrum agrees with the data from hadron-hadron scattering at an energy close to the ZEUS photon-proton c.m. energy. The diffractive slopes agree better with the hadronic data corresponding to a lower energy. In Fig. 2 the ZEUS diffractive points are plotted at 5 GeV and 10 GeV, the values of the invariant mass of the dissociated photon. A similar behaviour has been observed for the diffractive dissociation of protons, i.e. the scale of the fragmentation of the excited system is related to the invariant mass rather than to the total c.m. energy [22]. The dashed line in Fig. 2 is a parabola in $\log(s)$ and was fitted to all the hadron-hadron points to indicate the trend of the data. As one can see, our photoproduction results are consistent with the hadronic data.

The non-diffractive spectrum in Fig. 1 clearly departs from the exponential shape at high p_T values. Such a behaviour is expected from the contribution of the hard scattering of partonic constituents of the colliding particles, a process that can be described in the framework of perturbative QCD. It results in a high p_T behaviour of the inclusive spectrum that can be approximated by a power law formula:

$$\frac{1}{N_{ev}} \cdot \frac{d^2 N}{dp_T^2 d\eta} = A \cdot \left(1 + \frac{p_T}{p_{T0}}\right)^{-n} \quad (2)$$

where A , p_{T0} and n are parameters determined from the data. The fit to the ZEUS points in the region of $p_T > 1.2$ GeV gives a good description of the data and results in the parameter

values $p_{T0} = 0.54$ GeV, $n = 7.25$ and $A = 394$ GeV⁻². The statistical precision of these numbers is described by the covariance matrix shown in Table 5. The fitted function is shown in Fig. 1 as the dotted line.

In Fig. 3 the ZEUS data are presented together with the results of a similar measurement from the H1 collaboration at $\langle W \rangle = 200$ GeV [29] and the data from the WA69 photoproduction experiment at a c.m. energy of $\langle W \rangle = 18$ GeV [2]. For the purpose of this comparison, the inclusive cross sections published by those experiments were divided by the corresponding total photoproduction cross sections [30, 31]. Our results are in agreement with the H1 data. The comparison with the WA69 data shows that the transverse momentum spectrum becomes harder as the energy of the γp collision increases. Figure 3 also shows the functional fits of the form (2) to $p\bar{p}$ data from UA1 and CDF at various c.m. energies [27, 28]. Since the fits correspond to inclusive cross sections published by these experiments, they have been divided by the cross section values used by these experiments for the absolute normalization of their data. The inclusive p_T distribution from our photoproduction data is clearly harder than the distribution for $p\bar{p}$ interactions at a similar c.m. energy and in fact is similar to $p\bar{p}$ at $\sqrt{s} = 900$ GeV.

This comparison indicates that in spite of the apparent similarity in the low p_T region between photoproduction and proton–antiproton collisions at a similar c.m. energy, the two reactions are different in the hard regime. There are many possible reasons for this behaviour. Firstly, both of the $p\bar{p}$ experiments used for the comparison measured the central rapidity region ($|\eta| < 2.5$ for UA1 and $|\eta| < 1$ for CDF), while our data correspond to $0.8 < \eta_{c.m.} < 3.4$. Secondly, according to VDM, the bulk of the γp collisions can be approximated as an interaction of a vector meson V with the proton. The p_T spectrum of Vp collisions may be harder than $p\bar{p}$ at a similar c.m. energy, since the parton momenta of quarks in mesons are on average larger than in baryons. Thirdly, in the picture where the photon consists of a resolved part and a direct part, both the anomalous component of the resolved photon and the direct photon become significant at high p_T and make the observed spectrum harder compared to that of Vp reactions.

Figure 4 shows the comparison of our non–diffractive data with the theoretical prediction obtained recently from NLO QCD calculations [32]. The charged particle production rates in a non–diffractive event were converted to inclusive non-diffractive cross sections by multiplying by the non–diffractive photoproduction cross section of $\sigma_{nd}(\gamma p \rightarrow X) = 91 \pm 11 \mu\text{b}$ [6]. The theoretical calculations relied on the GRV parametrisation of the parton densities in the photon and on the CTEQ2M parametrisation for partons in the proton [33]. The NLO fragmentation functions describing the relation between the hadronic final state and the partonic level were derived from the e^+e^- data [34]. The calculation depends strongly on the parton densities in the proton and in the photon, yielding a spread in the predictions of up to 30% due to the former and 20% due to the latter. The factorization scales of the incoming and outgoing parton lines, as well as the renormalization scale, were set to p_T . The uncertainty due to the ambiguity of this choice was estimated by changing all three scales up and down by a factor of 2. The estimates of the theoretical errors were added in quadrature and indicated in Fig. 4 as a shaded band. The theoretical calculation is in good agreement with the ZEUS data.

10 Conclusions

We have measured the inclusive transverse momentum spectra of charged particles in diffractive and non–diffractive photoproduction events with the ZEUS detector. The inclusive transverse momentum spectra fall exponentially in the low p_T region, with a slope that increases slightly going from the non–diffractive to the diffractive collisions with the lowest M_X . The diffractive

slopes are consistent with hadronic data at a c.m. energy equal to the invariant mass of the diffractive system. The non-diffractive low p_T slope is consistent with the result from $p\bar{p}$ at a similar c.m. energy but displays a high p_T tail clearly departing from the exponential shape. Compared to photoproduction data at a lower c.m. energy we observe a hardening of the transverse momentum spectrum as the collision energy increases. The shape of our p_T distribution is comparable to that of $p\bar{p}$ interactions at $\sqrt{s} = 900$ GeV. The results from a NLO QCD calculation agree with the measured cross sections for inclusive charged particle production.

11 Acknowledgments

We thank the DESY Directorate for their strong support and encouragement. The remarkable achievements of the HERA machine group were essential for the successful completion of this work and are gratefully appreciated. We gratefully acknowledge the support of the DESY computing and network services. We would like to thank B.A. Kniehl and G. Kramer for useful discussions and for providing the NLO QCD calculation results.

References

- [1] T.H.Bauer et al., Rev. Mod. Phys. 50 (1978) 261.
- [2] OMEGA Photon Collab., R.J. Apsimon et al., Z. Phys. C43 (1989) 63.
- [3] NA14 Collab., E.Auge et al., Phys. Lett. 169B (1986) 163;
NA14 Collab., R.Barate et al., Phys. Lett. 174B (1986) 458.
- [4] J.K.Storow, J. Phys. G: Nucl. Part. Phys. 19 (1993) 1641.
- [5] T.J.Chapin et al., Phys. Rev. D31 (1985) 17.
- [6] ZEUS Collab., M. Derrick et al., Z. Phys. C63 (1994) 391.
- [7] The ZEUS Detector, Status Report, DESY(1993).
- [8] ZEUS Collab., M. Derrick et al., Phys. Lett. B293 (1992) 465.
- [9] C. Alvisi et al., Nucl. Instr. Meth. A305 (1991) 30.
- [10] N. Harnew et al., Nucl. Instr. Meth. A279 (1989) 290;
C.B. Brooks et al., Nucl. Instr. Meth. A283 (1989) 477;
B. Foster et al., Nucl. Phys. B, Proc. Suppl. B32 (1993) 181.
- [11] ZEUS Collab., M. Derrick et al., DESY 95-007, accepted by Z. Phys. C.
- [12] M. Derrick et al., Nucl. Instr. Meth. A309 (1991) 77;
A. Andresen et al., Nucl. Instr. Meth. A309 (1991) 101;
A. Bernstein et al., Nucl. Instr. Meth. A336 (1993) 23.
- [13] D. Kisielewska et al., DESY-HERA report 85-25 (1985);
J. Andruszkow et al., DESY 92-066 (1992);
K. Piotrkowski, PhD Thesis (Cracow, INP-Exp), 1993, DESY F35D-93-06.
- [14] B. Burow, PhD Thesis (University of Toronto), 1993, DESY F35D-94-01.
- [15] B.R. Webber, Ann. Rev. Nucl. Part. Sci. 36 (1986) 253;
G. Marchesini et al., Comput. Phys. Comm. 67 (1992) 465.
- [16] T. Sjöstrand, Z. Phys. C42 (1989) 301;
H-U. Bengtsson and T. Sjöstrand, Comput. Phys. Commun. 46 (1987) 43;
T. Sjöstrand, CERN-TH. 6488/92 (1992).
- [17] M. Glück, E. Reya and A. Vogt, Phys. Rev. D45 (1992) 3986.
- [18] A. D. Martin, W. J. Stirling and R. G. Roberts, Phys. Lett. B306 (1993) 145.
- [19] N.N. Nikolaev and B.G. Zakharov, Z. Phys. C53 (1992) 331;
P. Bruni et al., Proc. Workshop on Physics at HERA, DESY (1991) 363;
A. Solano, PhD Thesis (University of Torino), 1993.
- [20] P. Bruni and G. Ingelman, DESY 93-187, proceedings of the Europhysics Conf. on HEP, Marseille 1993.

- [21] R. Hagedorn, Riv. Nuovo Cim. 6 (1983) 1.
- [22] K. Goulianos, Phys. Rep. 101 (1983) 169;
C. Geich-Gimbel, Int. Jour. Mod. Phys. A4 (1989) 1527;
G. Giacomelli, Int. Jour. Mod. Phys. A5 (1990) 223.
- [23] J.V.Allaby et al., Fourth International Conference on High Energy Collisions, Oxford (April 1972).
- [24] E.W.Anderson et al., Phys. Rev. Lett. 19 (1967) 198.
- [25] C.W.Akerlof et al., Phys. Rev. D3 (1971) 645.
- [26] P. Capiluppi et al., Nucl. Phys. B70 (1974) 1.
- [27] UA1 Collab., C.Albajar et al., Nucl. Phys. B335 (1990) 261.
- [28] CDF Collab., F.Abe et al., Phys. Rev. Lett. 61 (1988) 1819.
- [29] H1 Collab., I.Abt et al., Phys. Lett. B328 (1994) 176.
- [30] H1 Collab., T.Ahmed et al., Phys. Lett. B297 (1992) 205.
- [31] H.Abramowicz, E.M.Levin, A.Levy and U.Maor, Phys. Lett. B269 (1991) 465.
- [32] F.M. Borzumati, B.A. Kniehl and G. Kramer, Z. Phys. C59 (1993) 341;
B.A. Kniehl and G. Kramer, Z. Phys. C62 (1994) 53.
- [33] J.F. Botts et al., Michigan State University Report, MSUHEP-93/28.
- [34] J. Binnewies, B.A. Kniehl and G. Kramer, DESY 94-124.

p_T [GeV]	$\frac{1}{N_{ev}} \cdot \frac{d^2N}{dp_T^2 d\eta}$ [GeV ⁻²]	σ_{stat} [GeV ⁻²]	σ_{syst} [GeV ⁻²]
0.30– 0.40	4.98	0.05	0.74
0.40– 0.50	2.99	0.03	0.44
0.50– 0.60	1.78	0.02	0.26
0.60– 0.70	1.09	0.01	0.16
0.70– 0.80	0.641	0.012	0.096
0.80– 0.90	0.420	0.010	0.063
0.90– 1.00	0.259	0.007	0.038
1.00– 1.10	0.164	0.005	0.024
1.10– 1.20	0.107	0.004	0.016
1.20– 1.30	0.0764	0.0034	0.0114
1.30– 1.40	0.0513	0.0017	0.0077
1.40– 1.50	0.0329	0.0012	0.0049
1.50– 1.60	0.0242	0.0010	0.0036
1.60– 1.70	0.0175	0.0008	0.0026
1.70– 1.80	0.0133	0.0006	0.0020
1.80– 1.90	0.0082	0.0005	0.0012
1.90– 2.00	0.00615	0.00038	0.00092
2.00– 2.14	0.00454	0.00028	0.00068
2.14– 2.29	0.00360	0.00024	0.00054
2.29– 2.43	0.00215	0.00017	0.00032
2.43– 2.57	0.00166	0.00013	0.00025
2.57– 2.71	0.00126	0.00012	0.00018
2.71– 2.86	0.00098	0.00010	0.00015
2.86– 3.00	0.000625	0.000071	0.000093
3.00– 3.25	0.000456	0.000048	0.000068
3.25– 3.50	0.000252	0.000031	0.000037
3.50– 3.75	0.000147	0.000020	0.000022
3.75– 4.00	0.000094	0.000012	0.000014
4.00– 4.50	0.000067	0.000008	0.000010
4.50– 5.00	0.0000301	0.0000045	0.0000045
5.00– 5.50	0.0000151	0.0000029	0.0000023
5.50– 6.00	0.0000082	0.0000021	0.0000012
6.00– 7.00	0.0000038	0.0000009	0.0000006
7.00– 8.00	0.0000014	0.0000005	0.0000002

Table 1: *The rate of charged particle production in an average non-diffractive event. The data correspond to $-1.2 < \eta < 1.4$. The σ_{stat} and σ_{syst} denote the statistical and systematic errors.*

p_T [GeV]	$\frac{1}{N_{ev}} \cdot \frac{d^2 N}{dp_T^2 d\eta}$ [GeV $^{-2}$]	σ_{stat} [GeV $^{-2}$]	σ_{syst} [GeV $^{-2}$]
0.30– 0.40	1.63	0.06	0.24
0.40– 0.50	1.02	0.04	0.15
0.50– 0.60	0.559	0.028	0.083
0.60– 0.70	0.308	0.019	0.046
0.70– 0.80	0.165	0.013	0.024
0.80– 0.90	0.088	0.011	0.013
0.90– 1.00	0.0479	0.0059	0.0071
1.00– 1.10	0.0312	0.0052	0.0046
1.10– 1.20	0.0196	0.0042	0.0029
1.20– 1.35	0.0100	0.0018	0.0015
1.35– 1.50	0.00304	0.00087	0.00045
1.50– 1.75	0.00153	0.00052	0.00023

Table 2: *The rate of charged particle production in an average event with a diffractively dissociated photon state of a mass $\langle M_X \rangle = 5$ GeV. The data correspond to $-1.2 < \eta < 1.4$. The σ_{stat} and σ_{syst} denote the statistical and systematic errors.*

p_T [GeV]	$\frac{1}{N_{ev}} \cdot \frac{d^2 N}{dp_T^2 d\eta}$ [GeV $^{-2}$]	σ_{stat} [GeV $^{-2}$]	σ_{syst} [GeV $^{-2}$]
0.30– 0.40	3.87	0.10	0.34
0.40– 0.50	2.32	0.06	0.20
0.50– 0.60	1.46	0.04	0.13
0.60– 0.70	0.803	0.033	0.072
0.70– 0.80	0.485	0.023	0.043
0.80– 0.90	0.288	0.017	0.025
0.90– 1.00	0.176	0.012	0.015
1.00– 1.10	0.109	0.009	0.009
1.10– 1.20	0.0732	0.0075	0.0065
1.20– 1.35	0.0294	0.0035	0.0026
1.35– 1.50	0.0186	0.0028	0.0016
1.50– 1.75	0.0086	0.0014	0.0008
1.75– 2.00	0.00260	0.00066	0.00023
2.00– 2.50	0.00076	0.00023	0.00007

Table 3: *The rate of charged particle production in an average event with a diffractively dissociated photon state of a mass $\langle M_X \rangle = 10$ GeV. The data correspond to $-1.2 < \eta < 1.4$. The σ_{stat} and σ_{syst} denote the statistical and systematic errors.*

sample	b [GeV $^{-1}$]	$\sigma_{stat}(b)$	$\sigma_{syst}(b)$	a	$\sigma_{stat}(a)$	$cov(a, b)$
non-diffractive	4.94	0.09	0.19	3.39	0.09	-0.011
diff $\langle M_X \rangle = 5$ GeV	5.91	0.17	0.19	2.78	0.10	-0.016
diff $\langle M_X \rangle = 10$ GeV	5.28	0.10	0.17	3.34	0.06	-0.006

Table 4: *The values of the parameters resulting from the fits of equation (1) to ZEUS data in the interval $0.3 < p_T < 1.2$ GeV. The σ_{stat} and σ_{syst} indicate the statistical and systematic errors.*

	p_{T0}	n	A
p_{T0}	$0.32 \cdot 10^{-3}$	$0.48 \cdot 10^{-3}$	$-0.10 \cdot 10^1$
n		$0.12 \cdot 10^{-2}$	$-0.12 \cdot 10^1$
A			$0.32 \cdot 10^4$

Table 5: *The covariance matrix corresponding to the fit of equation (2) to the non-diffractive data for $p_T > 1.2$ GeV.*

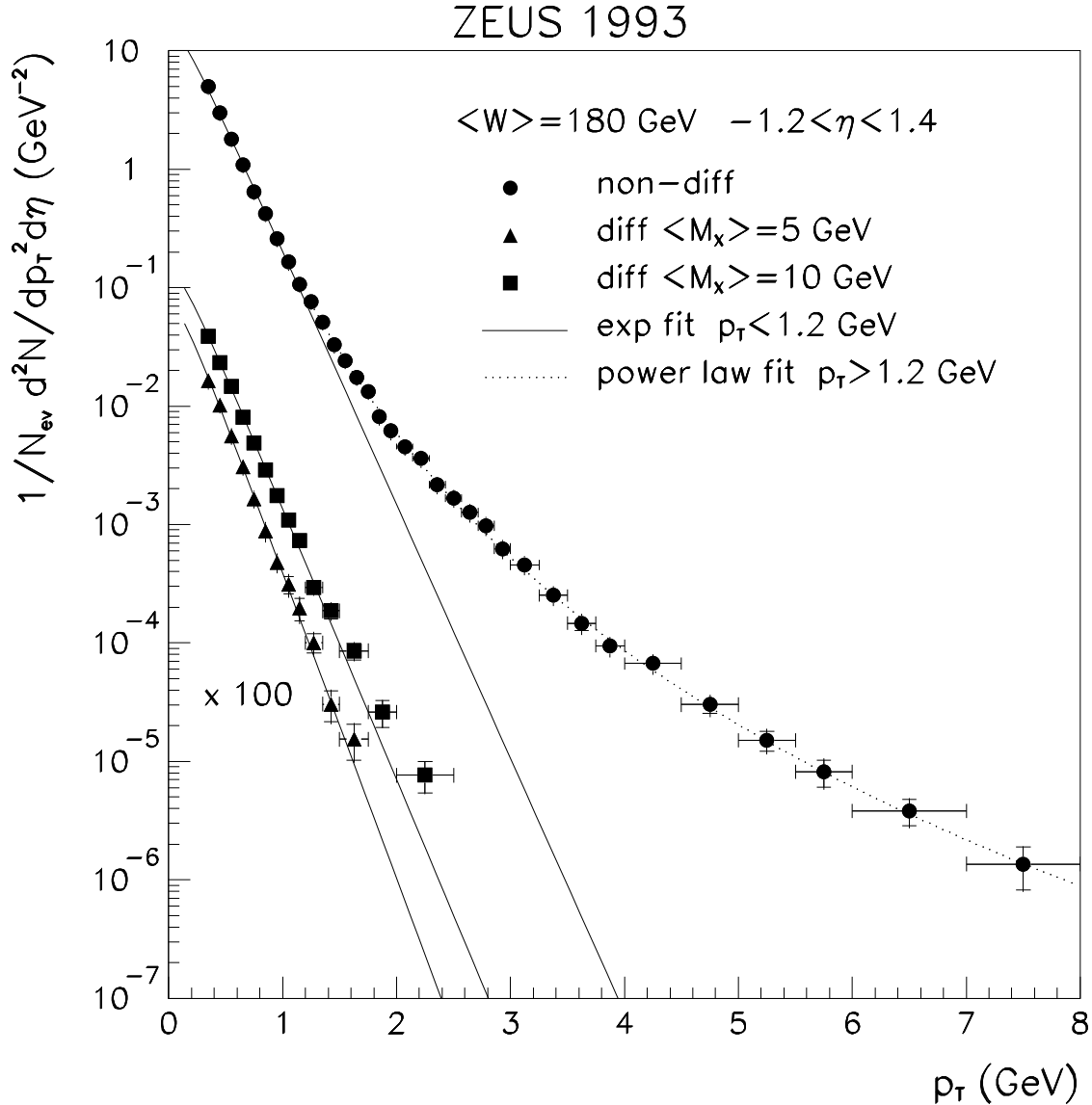


Figure 1: *Inclusive transverse momentum distributions of charged particles in photoproduction events at $\langle W \rangle = 180 \text{ GeV}$ averaged over the pseudorapidity interval of $-1.2 < \eta < 1.4$. The inner error bars indicate the statistical errors and the outer ones represent the quadratic sum of the statistical and systematic errors. Solid lines indicate fits of equation (1) to the data in the region of $p_T < 1.2 \text{ GeV}$. The dotted line shows a power law formulae (2) fitted to the non-diffractive data for $p_T > 1.2 \text{ GeV}$. For the sake of clarity the diffractive points are shifted down by two orders of magnitude.*

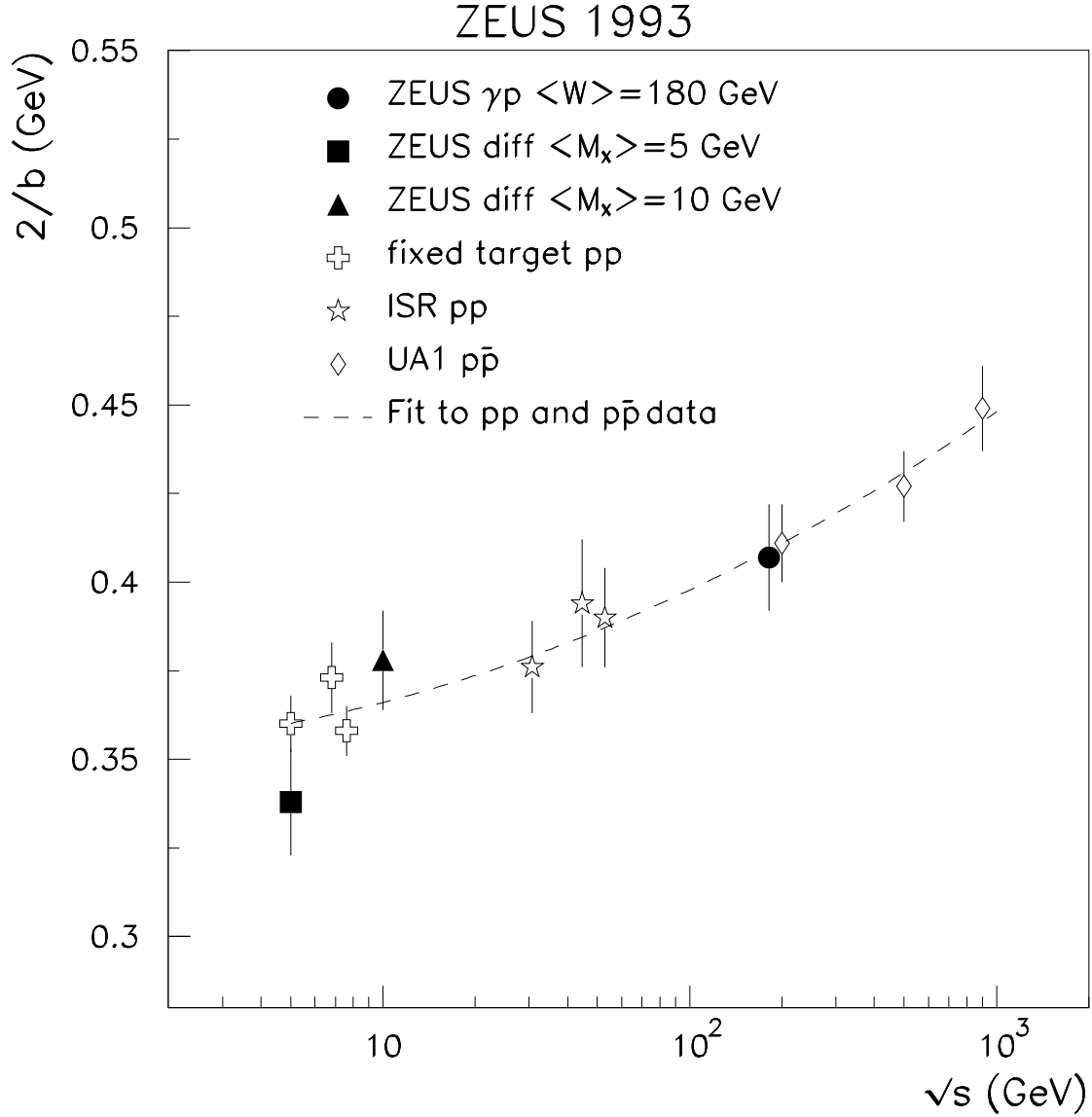


Figure 2: Inverse slope of the exponential fit of the form (1) vs. the c.m. energy for different experiments. The fixed target data were taken from [23] [24] [25], ISR – [26], UA1– [27]. The ZEUS non-diffractive point is placed at the photon-proton c.m. energy. The diffractive points are plotted at the energies corresponding to the mean value of the invariant mass $\langle M_X \rangle$. The error bars indicate the quadratic sum of the statistical and systematic errors. The dashed line is a parabola in $\log(s)$ and was fitted to all the hadron-hadron points to indicate the trend of the data.

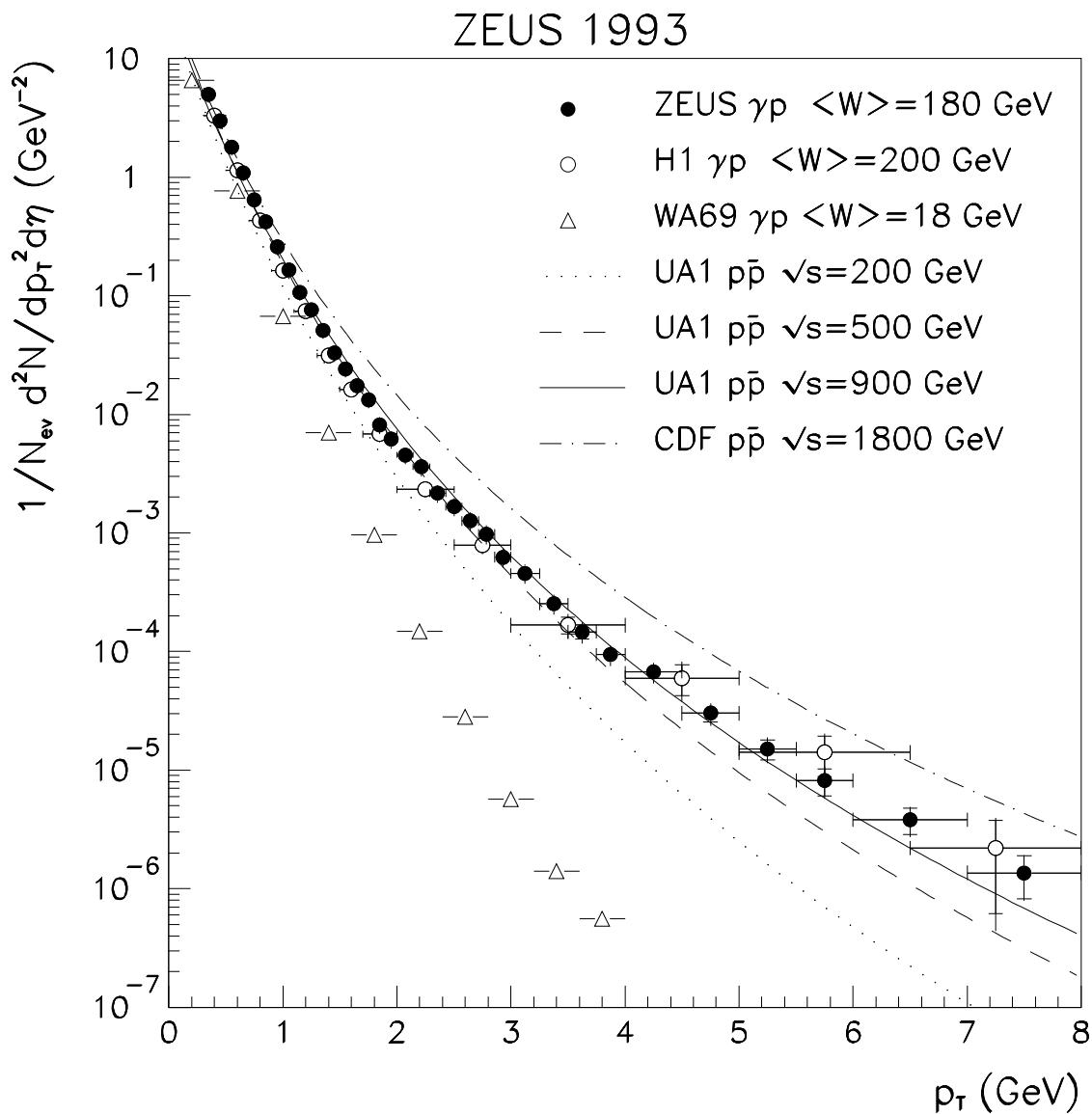


Figure 3: Comparison of ZEUS non-diffractive transverse momentum spectrum with the data from H1 [29], OMEGA [2], UA1 [27] and CDF [28]. The inner error bars indicate the statistical errors and the outer ones represent the quadratic sum of the statistical and systematic errors.

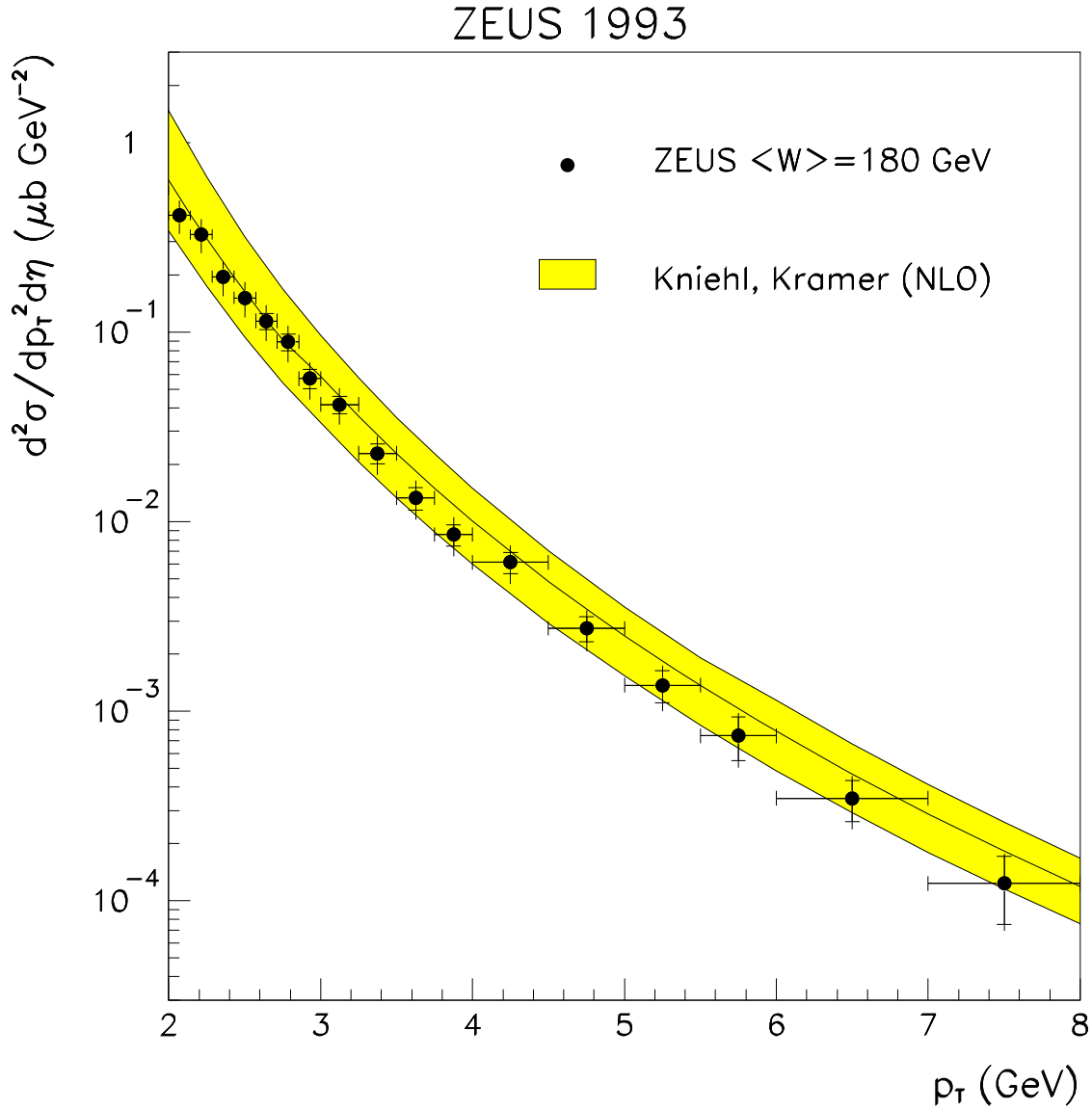


Figure 4: Comparison of the ZEUS inclusive cross sections for non-diffractive photoproduction at $\langle W_{\gamma p} \rangle = 180$ GeV with the NLO QCD calculation results from [32]. The inner error bars on the data points indicate the statistical errors and the outer ones represent the quadratic sum of the statistical and systematic errors. The shaded band corresponds to the uncertainty of the theoretical calculation.